A Numerical Exploration of Symmetry Breaking in Particle Systems

Directed Reading Program Report
Department of Mathematics and Statistics
McGill University

Charles-Étienne Lessard Miguel Ayala (Mentor)

May 2025

Abstract

We use numerical simulations to study a high-dimensional dynamical system that describes the gradient flow of an energy function defined on a system of particles. We investigate how the steady states exhibit a symmetry-breaking phenomenon. We implement these simulations in Julia, a language designed for scientific computing.

1 Introduction

The Directed Reading Program (DRP) offered by McGill's Department of Mathematics and Statistics pairs selected undergraduate students with graduate mentors to introduce them to mathematical research. Over the course of a semester, the undergraduate student explores a mathematical topic in depth, culminating in a short written report and a 10-minute oral presentation to fellow DRP participants and mentors. From January to May 2025, I had the opportunity to work with Miguel Ayala, a PhD student in the department, and explore computer-assisted proofs and computational methods in applied mathematics.

The main goal of our project was to understand how computers can aid in modern applied mathematical research. Scientific computing is a powerful tool that enables faster analysis and exploration of complex problems. It also plays a vital role in industry, where large datasets must be processed and analyzed efficiently. Computational methods in applied mathematics can be used to approximate solutions to complex systems of differential equations. They can also be used to filter, group, and compute summary statistics of large datasets, and to visualize the results in a clear and flexible way.

In this paper, we describe how we use computational tools to study the structure of local minimizers in a high-dimensional dynamical system. We begin by introducing the system's energy function, its gradient, and its Hessian. Then we describe how we use Julia to implement and solve the system of equations. The rest of the report analyzes a symmetry-breaking phenomenon in the structure of the steady states and shows how computational methods help analyze and visualize various properties of these shapes.

2 The Energy Function of a System of Particles

Consider a system of N particles $X_i \in \mathbb{R}^3$ $i = 1, \ldots, N$. The energy function of the particle system at each time is given by

$$E(X_1, \ldots, X_N) := \frac{1}{2N} \sum_{i \neq j} K_{\alpha,\lambda}(|X_i - X_j|) \tag{1}$$

or equivalently,

$$E(X_1, \ldots, X_N) := \frac{1}{N} \sum_{i=1}^{N} K_{\alpha,\lambda}(|X_i - X_j|)$$

where the interaction kernel is

$$K_{\alpha,\lambda}(r) := \frac{1}{\alpha} r^{\alpha} + \frac{1}{\lambda} r^{-\lambda} \tag{2}$$

with the attraction and repulsion parameters α and λ both being real positive numbers. This specific kernel came from this paper on nonlocal interaction energies [1].

Given two particles $X_1 = (x_1, y_1, z_1)$ and $X_2 = (x_2, y_2, z_2)$ in $\mathbb{R}^3$, we use the notation $|X_1 - X_2|$ for the Euclidean distance between the two particles:

$$|X_1 - X_2| := \sqrt{(x_1 - x_2)^2 + (y_1 - y_2)^2 + (z_1 - z_2)^2}$$

2.1 The Gradient and Hessian of the Energy Function

To find the steady states of the energy function, we track each particle X_i, for $i = 1, \ldots, N$ using the vector field given by the gradient of the energy:

$$\frac{dX_i}{dt} = -\nabla_{X_i} E(X) = -\frac{1}{N} \sum_{j=1}^{N} \nabla K_{\alpha,\lambda}(|X_i - X_j|) \tag{3}$$

Steady states occur when all particles stop moving, which corresponds to the vanishing of the gradient. For N particles, the gradient of the energy function will be a system of $3N$ ODEs. For example, suppose we have the particles X_1, X_2, X_3. Using Equation (3), if $X_1 = (x_1, y_1, z_1)$, we see that:

$$\frac{dX_1}{dt} = -\begin{bmatrix} \frac{\partial E}{\partial x_1} \\ \frac{\partial E}{\partial y_1} \\ \frac{\partial E}{\partial z_1} \end{bmatrix} = -\frac{1}{3} \begin{bmatrix} \frac{\partial (K_{\alpha,\lambda}(|X_1 - X_2|) + K_{\alpha,\lambda}(|X_1 - X_3|))}{\partial x_1} \\ \frac{\partial (K_{\alpha,\lambda}(|X_1 - X_2|) + K_{\alpha,\lambda}(|X_1 - X_3|))}{\partial y_1} \\ \frac{\partial (K_{\alpha,\lambda}(|X_1 - X_2|) + K_{\alpha,\lambda}(|X_1 - X_3|))}{\partial z_1} \end{bmatrix}$$

Following the definition for the interaction kernel of eq. (2), one can show that :

$$\frac{\partial K_{\alpha,\lambda}(|X_1 - X_j|)}{\partial x_1} = (x_1 - x_j)(r_{1j}^{\alpha-2} - r_{1j}^{-(\lambda+2)})$$

$$\frac{\partial K_{\alpha,\lambda}(|X_1 - X_j|)}{\partial y_1} = (y_1 - y_j)(r_{1j}^{\alpha-2} - r_{1j}^{-(\lambda+2)})$$

$$\frac{\partial K_{\alpha,\lambda}(|X_1 - X_j|)}{\partial z_1} = (z_1 - z_j)(r_{1j}^{\alpha-2} - r_{1j}^{-(\lambda+2)})$$

Let $X_i \in \mathbb{R}^3$ have coordinates (x_i, y_i, z_i). Denote the vector of 3 particles by

$$P = (x_1, x_2, x_3, y_1, y_2, y_3, z_1, z_2, z_3)$$

Then $\frac{dP}{dt} = -\nabla_p E$ will be a 9-dimensional vector. To implement and solve numerically for the steady states of the particle system, we also need to compute the Hessian of the energy function. Let $P = (x_1, x_2, ..., x_{3N})$ be the vector representing each coordinate of all the different particles. Then, the hessian of the energy function is defined by the following $3N \times 3N$ matrix:

$$H := \begin{pmatrix} \frac{\partial^2 E}{\partial x_1^2} & \frac{\partial^2 E}{\partial x_1 \partial x_2} & \cdots & \frac{\partial^2 E}{\partial x_1 \partial x_{3N}} \\ \frac{\partial^2 E}{\partial x_2 \partial x_1} & \frac{\partial^2 E}{\partial x_2^2} & \cdots & \frac{\partial^2 E}{\partial x_2 \partial x_{3N}} \\ \vdots & \vdots & \ddots & \vdots \\ \frac{\partial^2 E}{\partial x_{3N} \partial x_1} & \frac{\partial^2 E}{\partial x_{3N} \partial x_2} & \cdots & \frac{\partial^2 E}{\partial x_{3N}^2} \end{pmatrix} \tag{4}$$

For a system of 3 particles, the hessian will be a 9×9 matrix. The eigenvalues of the Hessian indicate the stability of the steady states. In our simulations, the eigenvalues of the Hessian are always positive, meaning we are always finding stable steady states, which are also local minimizers. In the following sections, the term *local minimizers* will be used to refer to the steady states of the particle system.

3 Solving the System for a Fixed Number of Particles

Consider the energy function defined in eq. (1) with 50 particles. This yields a system of 150 ODEs. Solving this system by hand is not practical. However, we can use a scientific programming language such as Julia to implement a numerical algorithm that allows a computer to solve the system with high accuracy. For our simulations we will be using the numerical algorithm TRBDF2. The solver combines an implicit Runge-Kutta formula using a trapezoidal rule step with a backward differentiation formula of order 2. More details about this numerical algorithm and its implementation are found in the following references: [2] [3].

We start by generating a random initial condition for our system of particles. Recall that the interaction kernel depends on two parameters: α and λ. We fix our kernel parameters to $\lambda = 0.01$ and $\alpha = 20$. Using our Julia implementation, we are able to find the following steady states with a sup-norm precision of the order of 10^{-7}.

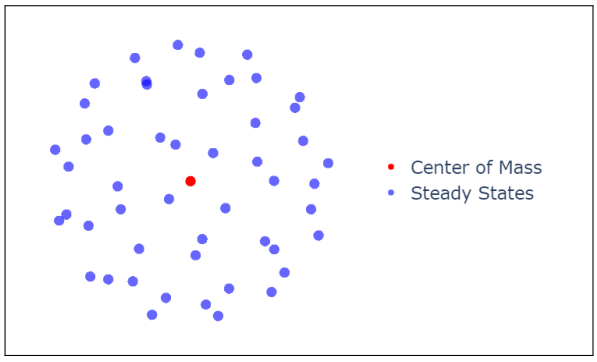

Figure 1: Position of the Local Minimizers when $\lambda = 0.01, \alpha = 20$

From the plot of fig. 1, it seems that the local minimizers replicate a spherical shape. What happens if we increase the parameter α?

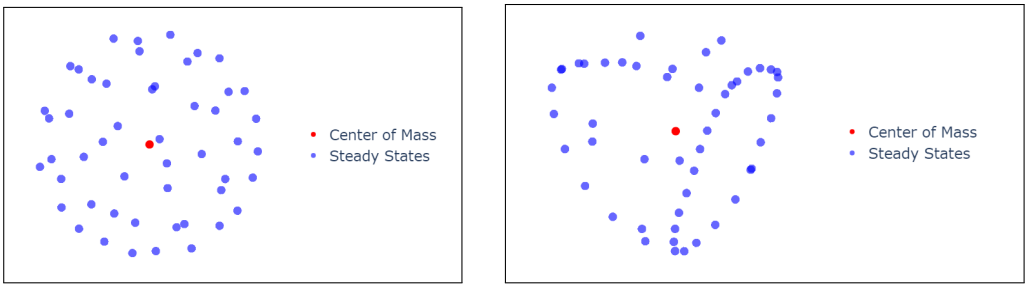

(a) $\lambda = 0.01$, $\alpha = 65$ (b) $\lambda = 0.01$, $\alpha = 70$

Figure 2: Comparison of the Shape of the Local Minimizers for $\alpha = 65$ and $\alpha = 70$ ($\lambda = 0.01$)

Comparing fig. 2 with fig. 1, we observe that between values 20 and 65, there is no significant qualitative change in the shape of the steady states. Radial symmetry is still present. However, between values 65 and 70, we observe a drastic change in shape-a clear break in radial symmetry. When $\alpha = 70$, the overall shape resembles a solid of constant width known as the *Meissner Body*. This resemblance becomes more apparent as we continue increasing α (see fig. 3 and fig. 4).

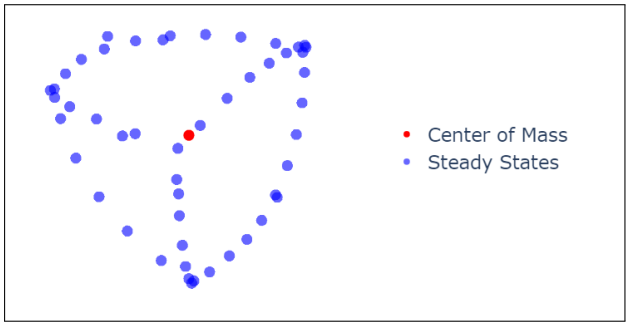

Figure 3: Local Minimizer for $\lambda = 0.01, \alpha = 200$

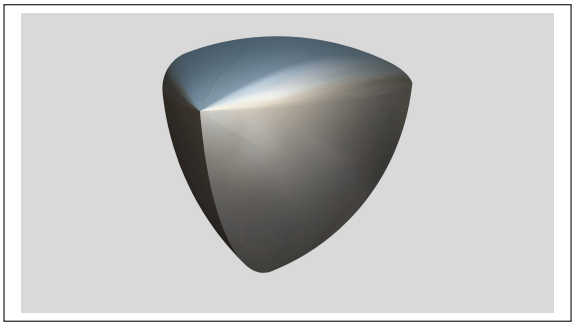

Figure 4: Meissner Body

How can we quickly identify the symmetry breaking without directly examining the shape of the local minimizers? How can we quantify the difference between the two shapes? In the first case, are we truly observing a sphere? In the second, does the shape genuinely resemble a solid of constant width? The following section introduces the tools needed to answer these questions.

4 Analyzing and Measuring the Shape of the Local Minimizers

We aim to quantify the overall shape of the local minimizers by examining various characteristics of the steady states and how they change as the parameter α is varied. For both types of shapes, we introduce specific distance-based measures that allow us to verify or reject the properties discussed in section 3.

4.1 Analyzing the Symmetry of the Local Minimizers

Let us begin by analyzing the overall shape of the global minimizers before the symmetry break. We define a reference frame with the origin at the center of mass of the steady states. If the configuration is truly spherical, we expect each local minimizer to lie at nearly the same distance from the center of mass. To test this, we measure the following quantities:

- Maximum distance between any steady state and the center of mass

- Minimum distance between any steady state and the center of mass
- Mean distance of all steady states from the center of mass
- Standard deviation of these distances

We let α range from 20 to 200 in steps of 5, keeping λ fixed at 0.01.

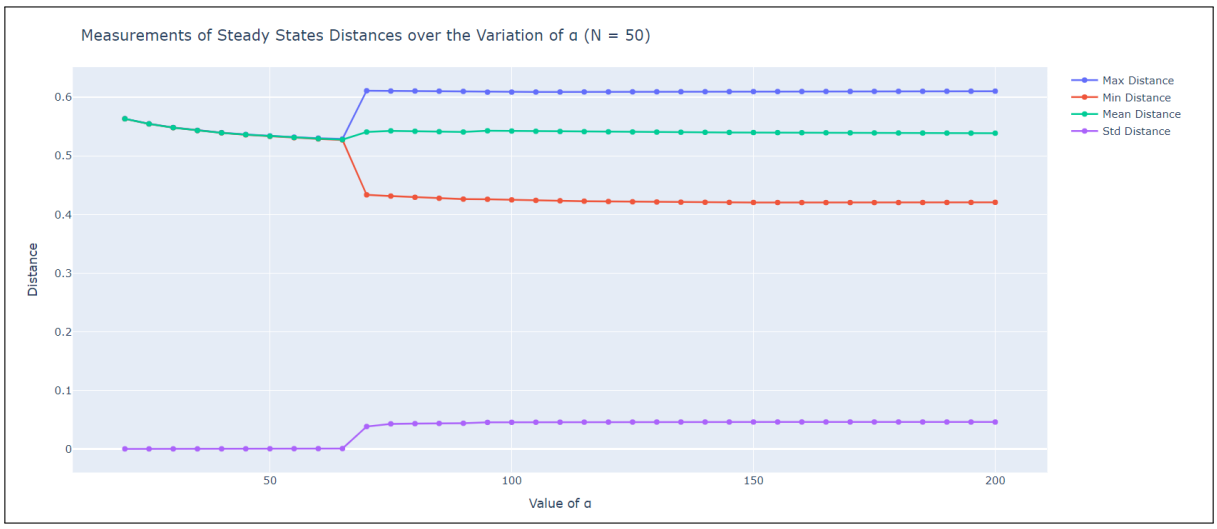

Figure 5: Evolution of the Maximum, Minimum, Mean and Standard Deviation of the Distances Measured Between Each Steady State and the Center of Mass ($\lambda = 0.01$, $\alpha \in [20; 200]$)

Distances from the Center of Mass for $\alpha = 20$

Maximum Distance	$563,4137 \times 10^{-3}$
Minimum Distance	$563,1221 \times 10^{-3}$
Mean Distance	$563,2145 \times 10^{-3}$
Standard Deviation	$9,383749 \times 10^{-5}$

From fig. 5 and its table we observe that for $\alpha = 20$ (before the symmetry breaking) the mean, maximum and minimum distances are all on the order of 10^{-3}. The standard deviation of all the distances between each local minimizer and the center of mass is on the order of 10^{-5}. This strongly suggests that the pattern observed in fig. 1 is indeed spherical.

4.2 Analyzing the Shape of the Local Minimizers After the Symmetry Break

We now turn to the shape observed after the symmetry break. We aim to determine whether it corresponds to a solid of constant width. A convex solid $S \subset \mathbb{R}^3$ has constant width w if for every pair of parallel planes tangent to the solid S, the distance between the two planes is always w [4]. Equivalently, the solid S is of constant width w if for any unit direction $\vec{u} \in \mathbb{R}^3$,

$$\max_{x \in S} \vec{u} \cdot x - \min_{x \in S} \vec{u} \cdot x = w$$

There exists an uncountable number of directions $\vec{u}$ in the unit sphere. However, sampling 500 random unit directions is sufficient to evaluate whether the shape is of constant width. Using the formula above, we compute a width w for each of the 50 particles in the system.

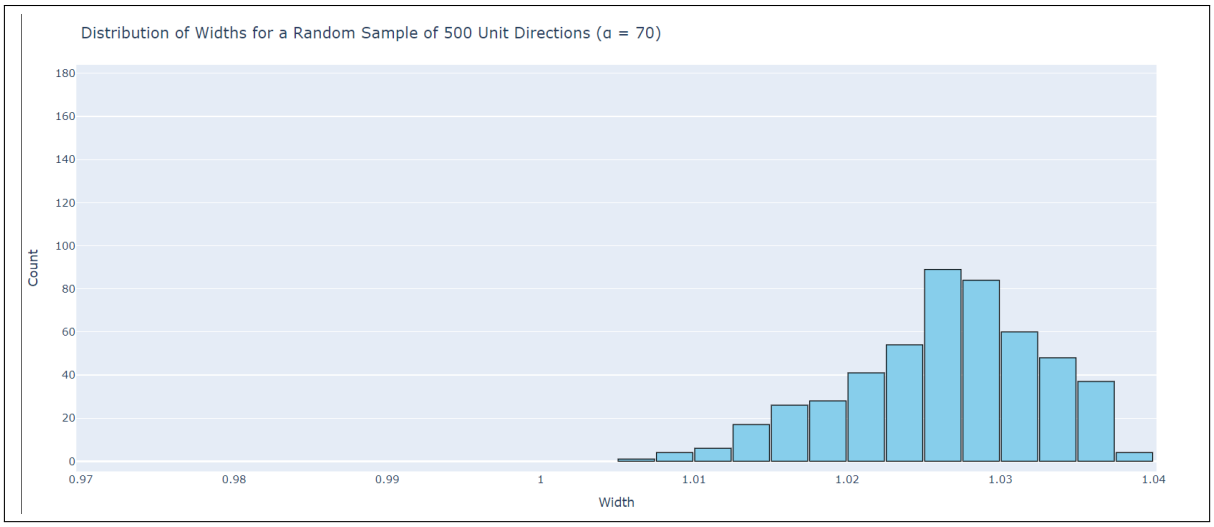

Figure 6: Distribution of the Solid Widths for 500 Different Directions when $\lambda = 0.01$, $\alpha = 70$

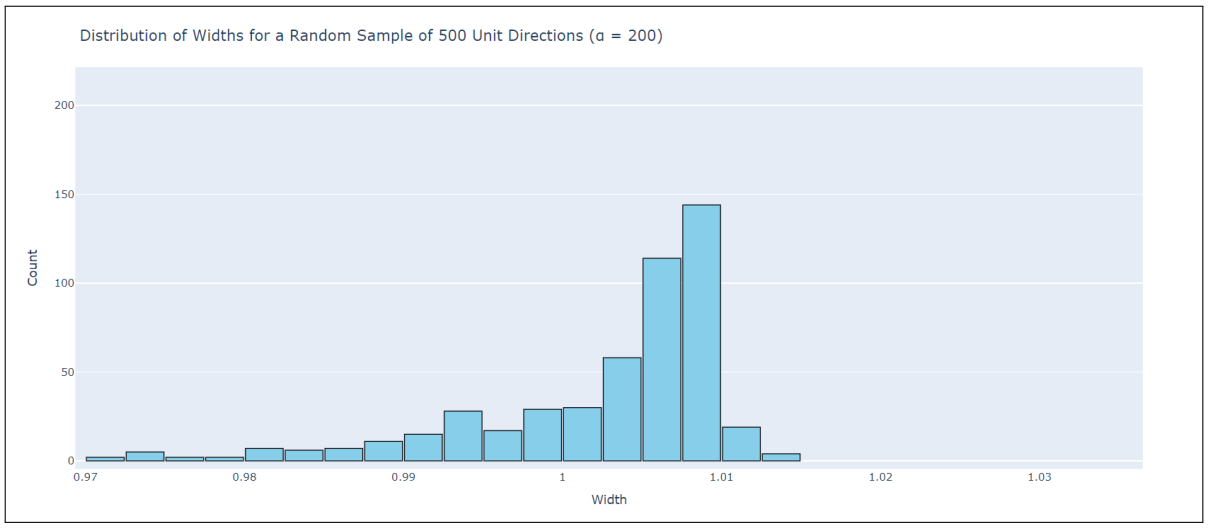

Figure 7: Distribution of the Solid Widths in 500 Different Directions when $\lambda = 0.01$, $\alpha = 200$

In both fig. 6 and fig. 7, it seems there is a small but non-negligible difference in the widths measured in the 500 different directions. In both cases, the standard deviation σ of the widths is close to 10^{-2}. This is significantly larger than the standard deviation reported in the table under fig. 5. However, since the distances measured and the algorithms used are different, we cannot directly compare these two standard deviations. The results from section 4.1 strongly suggest a spherical pattern for small values of α, and a sphere is a body of constant width. Interestingly, when we run this new algorithm with $\alpha = 20$, we also obtain a standard deviation σ close to 10^{-2}. This indicates the dispersion in the widths after the symmetry break is similar to the one observed before the symmetry break.

Another interesting phenomenon we notice is the influence of the attraction parameter α on the overall values of the computed widths. As α increases, all widths tend to decrease, indicating the particles are moving closer to the center of mass. This behaviour justifies the name *attraction* given to the parameter α.

5 Further Explorations

Up to now we only focused on the variation of the parameter α. However, we could also analyze the behavior of the local minimizers as we vary the parameter λ. Another interesting path is to investigate what happens when we increase the number of particles in our system. If we change the number of particles, do we arrive at the same conclusions as those discussed in section 4? To explore this, let us reproduce the diagram from fig. 5, this time for different values of N.

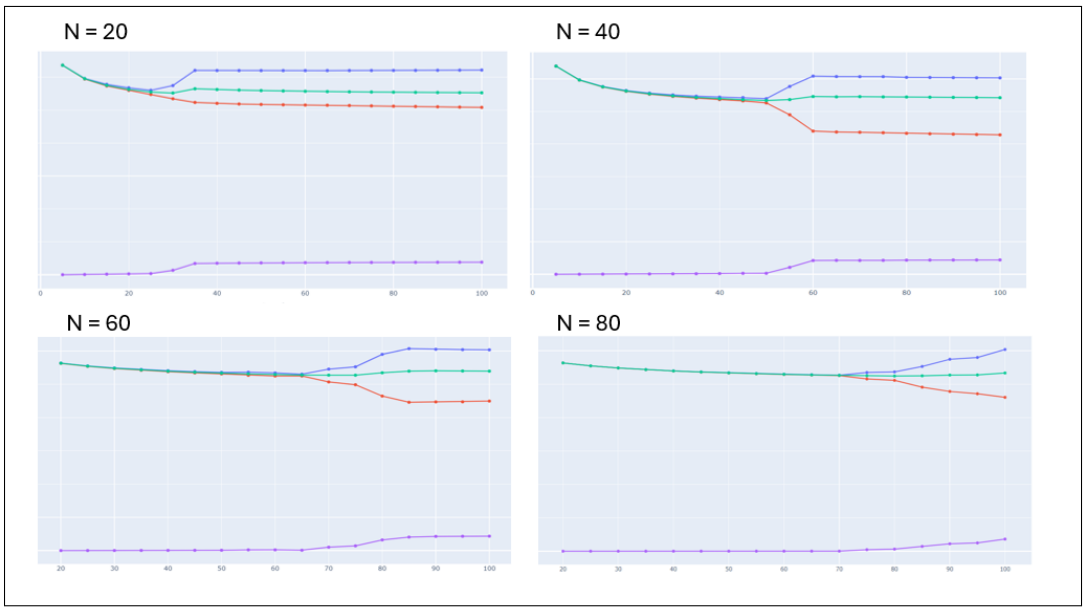

Figure 8: Evolution of the Local Minimizers Distances over a Fixed Range of α (20 to 100 with $\lambda = 0.01$) for Different Values of N

In fig. 8, we fixed the range of α between 20 and 100. When $N = 20$, the radial symmetry breaks between $\alpha = 20$ and $\alpha = 40$. When the number of particles is doubled to $N = 40$, the critical value of α shifts to around 55. Finally, when the number of particles is doubled again to $N = 80$, the symmetry break does not occur before $\alpha = 80$. Increasing the number of particles delays the start of symmetry breaking in the system.

6 Conclusion

In the previous sections, we have employed various visualization tools—such as scatter plots, line diagrams, and histograms—to illustrate our results. The use of the numerical algorithm TRBDF2, along with its Julia implementation, was also essential to the success of our simulations. These tools and techniques represent just a glimpse of the vast possibilities that computers offer in applied mathematical research and industry. As the complexity of the mathematical models we study continues to grow, the role of computational methods will become increasingly central. Mastering the ability to harness computational power, interpret the results effectively, and communicate them clearly will be a crucial skill for both current and future applied mathematicians.

References

[1] Almut Burchard, Rustum Choksi, and Elias Hess-Childs. On the strong attraction limit for a class of nonlocal interaction energies. *Nonlinear Analysis*, 198:111844, 2020.

[2] E. Hosea, M. and F. Shampine, L.˙ Analysis and implementation of tr-bdf2. *Applied Numerical Mathematics*, 20(1-2):21–37, 1996.

[3] Randolph E. Bank, Jr. Coughran, William M., Wolfgang Fichtner, Eric H. Grosse, Donald J. Rose, and R. Kent Smith. Transient simulation of silicon devices and circuits. *IEEE Transactions on Computer-Aided Design of Integrated Circuits and Systems*, 4(4):436–451, 1985.

[4] Thomas Lachand-Robert and Edouard Oudet. Bodies of constant width in arbitrary dimension. *Mathematische Nachrichten*, 280(7):740–750, 2007.